光学学报

匹配干涉结构对远程光纤传感系统噪声的影响

唐启永[1*]，曹春燕[2**]，夏兴宇[1]，刘国彬[1]，赵凡[1]，盛靖超[1]，郭金溢[1]

[1]中国人民解放军63893部队，河南 洛阳 471000；

[2]国防科技大学气象海洋学院，湖南 长沙 410073

摘要 研究了采用内调制相位产生载波(PGC)解调的匹配干涉型光纤传感系统中匹配干涉结构对传输光纤拾音噪声的影响。结果表明：当补偿干涉仪与传感部分相邻时，光学微分效应的作用可大幅度降低由传输光纤光路拾音引入的相位调制噪声；匹配光程差的增加不仅加剧了光频噪声向相位噪声的转换，同时也会影响相位调制噪声的转换幅度。通过设计合适的匹配光程差，并将补偿干涉仪进行有效屏蔽后与传感部分相邻放置，可以有效减小系统的相位噪声。研究成果为光纤传感远程传输系统的综合设计及噪声抑制技术提供了理论及实验基础，具有一定的参考意义。

关键词 光纤光学；光纤传感；匹配干涉；匹配光程差；相位调制噪声

中图分类号 TP253 **文献标志码** A **DOI：** 10.3788/AOS221071

1 引 言

干涉型光纤传感器基于光束干涉原理，具有工作频带宽、体积小、不易受电磁干扰等优点，对于维护国家安全，开发海上石油、天然气，地震探测告警等具有重要意义。实用化的光纤传感器多采用Mach-Zehnder型和Michelson型干涉仪结构[1]。其中匹配干涉型在线迈克耳孙光纤传感系统以其结构简单、光能利用率高、解调方案灵活等优点，成为研究热点之一[2]。

匹配干涉型光纤传感系统的工作原理是：光源输出的连续光经过声光调制器(AOM)后成为脉冲光，之后注入到补偿干涉仪(CMI)。入射脉冲在补偿干涉仪中反射，形成两个脉冲光，经光隔离器进入传感器。由补偿干涉仪返回的一系列脉冲经传感器后，其前一个脉冲经传感器长臂反射的光与后一个脉冲经短臂反射的光在时序上重叠干涉。匹配干涉仪的主要作用是实现光路匹配。干涉脉冲携带传感信息，经光电探测器、模/数转换以及信号解调后，获取外界信号。国外对匹配干涉型光纤传感系统的研究主要集中于基元技术、复用技术、信号检测技术[3-6]。国内Zhou等[7]采用非平衡迈克耳孙干涉仪，研究了窄线宽光纤激光器和激光二极管的相位噪声。结果表明，这两种激光器在臂差长于10 m和短于10 m时表现出不同的相位噪声特性。文献[8]研究了匹配干涉型光纤水听器阵列远程传输的噪声特性，对其中的相位调制噪声进行了一定的理论分析，并采用基于参考基元的解调算法对传输光纤的相位调制噪声进行抑制。文献[9-10]总结了我国光纤传感的发展历程、技术现状、面临的主要问题及发展前景。文献[11]从光纤水听器的主要发展方向、关键技术、新型光纤水听器三个层面介绍了光纤水听器技术。文献[12]分析了多种海水温盐深传感器的测量方法与实验结果，指出了技术上的优缺点，展望了光纤传感器在物理海洋观测领域的发展前景。在已有的国内外文献中，补偿干涉仪通常位于光发射端或光接收端，补偿干涉仪位于传感器端的研究较少，该结构应用于远程传输光纤传感系统时存在以下问题：1)传输光纤的光路拾音噪声不断累积，将在系统中引入较大的相位噪声[2]；2)在远程传输系统中，受激布里渊(SBS)效应对传输距离和系统噪声影响较大，需要采用非等程差的光频调制或参数匹配相位调制(PM)对SBS进行抑制[13-17]。然而，传统的匹配干涉结构通常是基于等程差干涉的，因此调制载波信号不能直接加载到干涉仪中，这意味着传统的匹配干涉结构方案不再适用。当然，载波信号可以通过压电换能器(PZT)或电光调制器(EOM)加载到干涉仪的一个臂上，但这样会破坏系统的全光特性，也会引入一些电噪声，因此原有等程差匹配方案不再适用。

针对以上问题，本文基于相位产生载波(PGC)解调的匹配干涉型光纤传感远程传输系统，首先分析了补偿干涉仪不同位置对系统相位调制噪声的影响，通过数值仿真和实验验证获得了最优的匹配干涉系统结

收稿日期： 2022-05-06；**修回日期：** 2022-06-21；**录用日期：** 2022-07-18；**网络首发日期：** 2022-07-28

基金项目： 国家自然科学基金(61605244，11574397)

通信作者： *812953295@qq.com；**ccy_nudt@163.com

构，其次研究了不同匹配光程差对系统相位调制噪声的影响，最后实验测量了不同匹配光程差时的相位噪声本底。匹配光程差指的是补偿干涉仪臂差与传感器臂差的光程差。本文所得结论对匹配干涉型光纤传感远程传输系统的设计及应用具有一定的指导意义。

2 理论分析

在干涉型光纤传感系统中，相位噪声决定着系统的检测灵敏度，是决定系统性能的关键参数之一。相位噪声的主要来源包括激光器强度与频率抖动、光纤传输过程中的瑞利散射与双重瑞利散射、放大器自发辐射、偏振漂移、非线性效应、环境扰动、电路噪声等。远程匹配干涉型光纤传感系统的传输光纤通常暴露在复杂的外界环境中，当受到周期性应力作用时，光纤的长度发生变化，从而使在其中传输的激光的相位受到调制，在系统中引入相位调制噪声[2]。如图 1 所示，匹配干涉系统通常分为两部分[18-19]：一部分是补偿干涉仪，位于发射端或接收端；另一部分是迈克耳孙干涉仪或时分复用阵列，位于传感端。为便于分析相位调制噪声与匹配干涉系统结构的关系，实验中在压电陶瓷上缠绕一定长度的光纤，当在压电陶瓷上施加余弦电压信号时，可以通过改变光纤的长度，实现对光纤中激光相位的调制，模拟环境扰动引起的相位调制噪声。假设作用于传输光纤上的调相噪声为单频余弦信号，设噪声为$f(t)=A\cos[\omega_n+\varphi(t)]$，其中噪声幅度为$A$，角频率为$\omega_n$，初相位为$\varphi(t)$。设单频光源光场为$E_1=2E_0\exp(\mathrm{j}\omega t)$，其中光源振幅为$2E_0$，角频率为$\omega$，j 为虚数单位。$L_1$、$L_2$分别为补偿干涉仪和传感器的臂差，二者的匹配光程差为$\Delta l=2n(L_1-L_2)$，$\tau_1=2nL_1/c$，$\tau_2=2nL_2/c$，$\tau=\tau_1-\tau_2=2n\Delta l/c$，$n$ 为光纤折射率，c 为真空中光速，理论分析中不考虑损耗的影响。

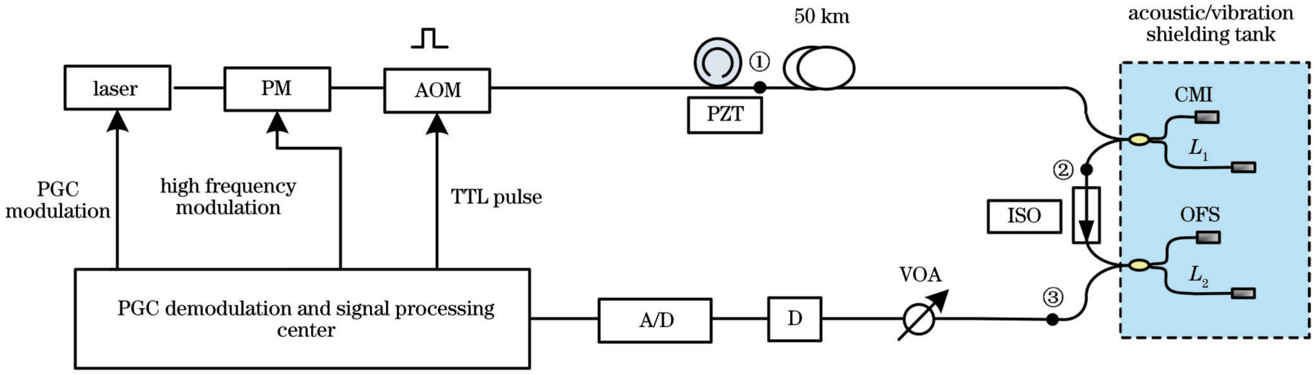

AOM: acoustic optical modulator; PM: phase modulation; PZT: piezo-electric transducer; ISO: isolator;
CMI: compensating Michelson interferometer; OFS: optical fiber sensor; VOA: variable optical attenuator;
A/D: analog-digital conversion; D: detector; TTL: transistor-transistor logic

图 1　噪声测试系统结构示意图

Fig. 1　Schematic diagram of noise testing system

2.1 紧凑匹配干涉结构

紧凑匹配干涉结构的补偿干涉仪和传感器相邻，此时相当于 PZT 和传输光纤位于图 1 中①位置处，匹配光程差为$\Delta l=2n(L_1-L_2)$，则补偿干涉仪的输出光场可以表示为

$$\begin{cases} E_1=E_0\exp\left\{\mathrm{j}\left[\omega t+A\cos\omega_n t+\varphi(t)\right]\right\} \\ E_2=E_0\exp\left\{\mathrm{j}\left[\omega(t-\tau_1)+A\cos\omega_n(t-\tau_1)+\varphi(t-\tau_1)\right]\right\} \end{cases}。\tag{1}$$

经传感器后相互干涉的两信号光场为

$$\begin{cases} E_1'=\dfrac{E_0}{2}\exp\left\{\mathrm{j}\left[\omega(t-\tau_2)+A\cos\omega_n(t-\tau_2)+\varphi(t-\tau_2)\right]\right\} \\ E_2'=\dfrac{E_0}{2}\exp\left\{\mathrm{j}\left[\omega(t-\tau_1)+A\cos\omega_n(t-\tau_1)+\varphi(t-\tau_1)\right]\right\} \end{cases}。\tag{2}$$

E_1'和E_2'发生干涉后的光强可以表示为

$$I=\frac{1}{2}E_0^2\left\{1+\cos\left[\omega\tau+\varphi(t)-\varphi(t-\tau)+A\cos\omega_n t-A\cos\omega_n(t-\tau)\right]\right\}=\frac{1}{2}E_0^2\left[1+\cos(\omega\tau+\Delta\phi_0+\Delta\phi_{n1})\right],\tag{3}$$

式中：$\Delta\phi_0=\varphi(t)-\varphi(t-\tau)$；$\Delta\phi_{n1}=A\cos(\omega_n t)-A\cos[\omega_n(t-\tau)]=-2A\sin\left[\omega_n\left(t-\frac{\tau}{2}\right)\right]\sin\frac{\omega_n\tau}{2}$。

2.2 分离匹配干涉结构

分离匹配干涉结构的补偿干涉仪和传感器隔开，此时相当于PZT和传输光纤位于图1中②位置处，激光脉冲经补偿干涉仪后分裂成两个脉冲。在传输光纤中，第一个脉冲传感到的是t时刻的噪声，而第二个脉冲传感的是$t+\tau_1$时刻的噪声，经传感器后相互干涉的两信号光场为

$$\begin{cases}E_1''=\dfrac{E_0}{2}\exp\left\{\mathrm{j}\left\{\omega(t-\tau_2)+A\cos\left\{\omega_n\left[t-(\tau_1-\tau_2)\right]\right\}+\varphi(t-\tau_2)\right\}\right\}\\ E_2''=\dfrac{E_0}{2}\exp\left\{\mathrm{j}\left\{\omega(t-\tau_1)+A\cos\left[\omega_n(t-\tau_1)\right]+\varphi(t-\tau_1)\right\}\right\}\end{cases}。\tag{4}$$

E_1''和E_2''发生干涉后的光强可以表示为

$$I=\frac{1}{2}E_0^2\left\{1+\cos\left\{\omega\tau+\varphi(t-\tau_1)-\varphi(t-\tau_2)+A\cos\omega_n\left[t-(\tau_1-\tau_2)\right]-A\cos\omega_n(t-\tau_1)\right\}\right\}=\frac{1}{2}E_0^2\left[1+\cos(\omega\tau+\Delta\phi_0+\Delta\phi_{n2})\right],\tag{5}$$

式中：$\Delta\phi_0=\varphi(t-\tau_2)-\varphi(t-\tau_1)$；$\Delta\phi_{n2}=A\cos\left\{\omega_n\left[t-(\tau_1-\tau_2)\right]\right\}-A\cos\left[\omega_n(t-\tau_1)\right]=-2A\sin\left[\omega_n\left(t-\frac{\tau_2}{2}\right)\right]\sin\frac{\omega_n\tau_2}{2}$。

通常情况下$\omega_n<2\pi\times10\ \mathrm{kHz}$，$\tau$、$\tau_1$、$\tau_2$小于1 μs（例如补偿干涉仪臂差$L_1=27.07\ \mathrm{m}$、传感器臂差$L_2=26.16\ \mathrm{m}$、$L_1-L_2<1\ \mathrm{m}$）。因此$\frac{\omega_n\tau}{2}$、$\frac{\omega_n\tau_2}{2}\ll1$，$\Delta\phi_{n1}$的幅度可进一步简化为$A\omega_n\tau$，$\Delta\phi_{n2}$的幅度可进一步简化为$A\omega_n\tau_2$。对比$\Delta\phi_{n1}$和$\Delta\phi_{n2}$可知，噪声幅度抑制程度为$20\lg(\tau_2/\tau)$。

2.3 不同臂差对噪声的影响

PGC调制解调方法需要施加一个调制载波信号，将要探测的信号加载到调制载波的边带上。调制载波有两种加载方式：内调制与外调制。内调制指的是通过直接调制激光器输出频率来施加PGC载波的方法，这种方法便于实现系统全光和阵列复用，故远程大规模阵列系统中常用这种方法。PGC调制载波产生的相位信号$\Delta\phi(t)$可表示为：$\Delta\phi=\frac{2\pi D}{c}\Delta\nu\cos\left[\omega_m(t)\right]=C\cos\left[\omega_m(t)\right]$，其中$C$为调制深度，$\omega_m$为调制频率，$\Delta\nu$为最大调制电压时的频移，$D$为干涉仪两臂光程差。根据PGC调制解调原理，最合适的调制深度为2.4，因此在PGC内调制中，要求干涉仪两臂的光纤长度不相等，使其满足$C=2.4$[20]。

激光器的相位噪声与干涉仪的臂差的关系[21]为$\Delta\phi=\frac{2\pi D}{c}\Delta\mu$，其中$\Delta\mu$为激光器线宽。激光器的相位噪声与激光器线宽成正比，与干涉仪光程差成正比。所以，在实际的远程干涉型光纤传感系统中，往往采用窄线宽激光器（约kHz量级）获得较小的相位噪声本底。然而，在远程干涉型光纤传感系统中，激光器的窄线宽往往会导致各种非线性效应阈值的降低，在50 km远程干涉型光纤传感系统中SBS阈值小于5 mW，当E_2''发生时，相当一部分的光功率转化为后向斯托克斯光，导致接收端光功率明显下降，同时相位噪声与强度噪声明显增加，系统性能明显下降。采用相位调制抑制远程干涉型光纤传感系统SBS效应及相位噪声时，要求干涉仪臂差满足[17] $\omega_p\Delta t=2k\pi$（$k=1,2,3,\cdots$），其中ω_p为相位调制频率，$\Delta t=D/c$。

由理论分析可得，当补偿干涉仪与传感器相邻时，相位调制噪声幅度与补偿干涉仪和传感器的匹配效果有关。这种结构的微分作用对相位调制噪声有一定程度的削弱，且匹配光程差越小，抑制效果越好；对于返回传输光纤上的相位调制噪声，即PZT位于③位置处，噪声作用于干涉后的脉冲，解调时可以消除，因此不会产生影响。当补偿干涉仪与传感器隔开时，相位调制噪声幅值仅与传感器的臂差相关，臂差越大，相位调制噪声越大，与补偿干涉仪的臂差或匹配光程差无关，两种结构下的系统相位调制噪声幅度差为$20\lg(\tau_2/\tau)$。

3 实验与分析

3.1 实验设计

利用图1所示的测试系统，将补偿干涉仪和传感器置于真空屏蔽桶内，屏蔽桶内外粘贴减振材料，以抑制外界环境噪声。干涉仪输出由探测器（D）探测并经数字采集卡（A/D）将模拟信号转化为数字信号，经计算机（PC）PGC解调程序获得相位变化信息和相应的外界信号，可变光衰减器（VOA）用于调节进入探测器的功率。相位调制用于抑制SBS效应，PZT直径为

6 cm，上面缠绕约5 m长的光纤，由信号发生器驱动，用于模拟传输光纤上的相位调制噪声，信号频率为2 kHz，传输光纤长50 km。系统采用的光源为单频窄线宽半导体激光器（RIO ORION™ Series，≈3 kHz@1550 nm），波长为1550 nm，线宽小于10 kHz，AOM频率为480 kHz，探测器带宽为10 MHz，采样率为480 kHz，PGC调制频率为30 kHz。

3.2　臂差相同、补偿干涉仪位置不同

补偿干涉仪的臂差为27.07 m，光纤传感器的臂差为26.16 m，图2中菱形+实线和方形+实线分别为补偿干涉仪与传感器相邻和分开的实验结果，星形+虚线为相邻时的实验结果加上29.2 dB，横坐标为PZT上的电压。对以上不同结构引入传输光纤上的相位调制噪声进行分析，其中噪声差异主要来源于补偿干涉仪的27.07 m臂差和传感器的26.16 m臂差的匹配效果。当补偿干涉仪与传感器相邻时，取光纤折射率$n=1.5$，此时的匹配光程差为2.73 m；当补偿干涉仪与传感器分开时，匹配光程差为78.48 m。上述两种不同结构在传输线路上引入的相位调制噪声相差约为28.9 dB，与理论差值29.2 dB符合得较好。由于补偿干涉仪与传感器相邻结构的微分作用，相位调制噪声在一定程度上被削弱。且由式(3)可知，匹配光程差越小，微分作用越明显。

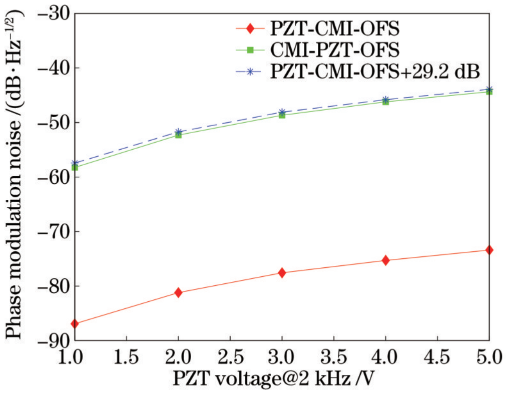

图2　不同匹配干涉结构的相位调制噪声对比图

Fig. 2　Comparison of phase modulation noise for different matching interference structure

3.3　补偿干涉仪位置不变、臂差改变

实验中进一步测试了补偿干涉仪与传感器分开结构下，不同臂差时的相位调制噪声，如图3所示。图中星形+实线表示补偿干涉仪臂差保持26.16 m不变、传感器臂差从26.06 m逐步增加到39.40 m的相位调制噪声，圆圈+实线表示补偿干涉仪臂差从26.06 m逐步增加到39.40 m、传感器臂差保持26.16 m不变时的相位调制噪声。

从图3中可以看出，随着传感器臂差的增大，相位调制噪声逐渐增大（从−58.17 dB增加到−54.40 dB）。当传感器臂差为26.16 m保持不变时，相位调制噪声的最大值为−58.22 dB，最小值为−58.44 dB，相差0.23 dB，平均值为−58.29 dB，说明此时噪声幅度基本不变。

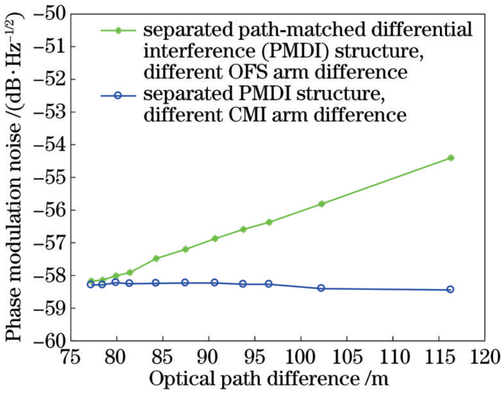

图3　不同匹配光程差时的相位调制噪声对比图

Fig. 3　Comparison of phase modulation noise for different optical path difference

上述两组实验表明：当补偿干涉仪与传感器分开时，相位调制噪声仅与传感器的臂差有关，臂差越大，相位调制噪声越大，与匹配干涉仪的臂差无关，与二者的匹配光程差也无关，该结果与理论分析相符。

3.4　对低频随机噪声的抑制

由以上分析可知：当补偿干涉仪与传感器分开时，相位调制噪声较大；当补偿干涉仪与传感器相邻时，噪声明显减小，这种结构对随机噪声同样有抑制作用。如图4所示，以58.59 Hz频点为例，其噪声分别为−58.16 dB和−89.11 dB，二者相差30.95 dB，与理论差值29.2 dB相近。

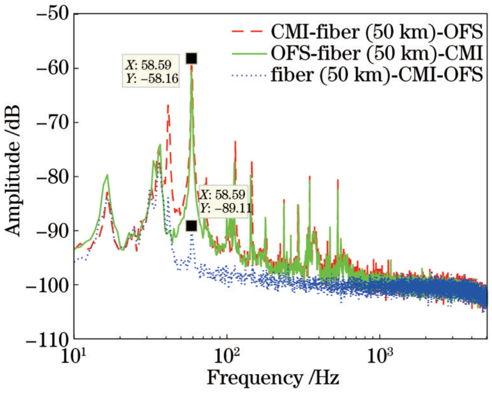

图4　对低频随机噪声的抑制

Fig. 4　Suppression of low-frequency random noise

3.5　返回传输光纤上的相位调制噪声

图5为PZT在图1中③位置处的实验结果，对比PZT在图1中①位置处的结果（图6），可以看出，返回传输光纤的相位调制噪声在解调过程中可以被消除，与理论分析一致。图例“26.06-32.71-PZT-1v”的意思是补偿干涉仪和传感器的臂差分别为26.06 m、32.71 m，PZT位于返回传输光纤，加载的电压为1 V；

其他图例同理。

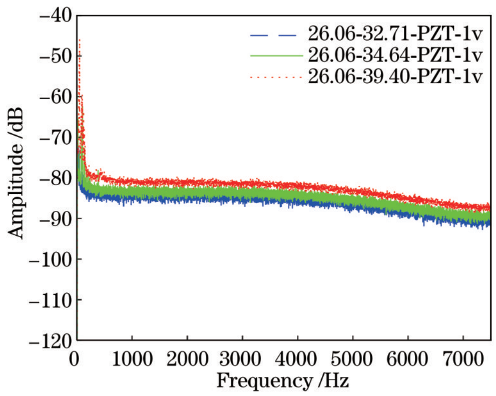

图 5　PZT 在图 1 中③位置处的实验结果

Fig. 5　Experimental results of PZT at position ③ in Fig. 1

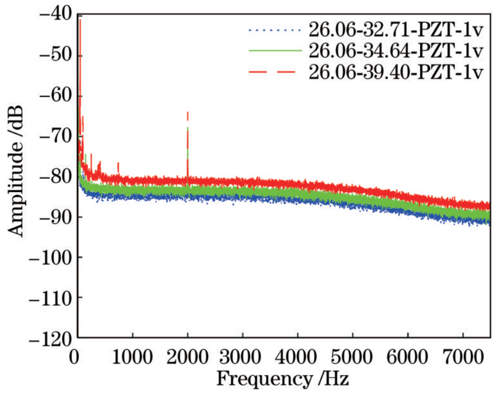

图 6　PZT 在图 1 位置①处的实验结果

Fig. 6　Experimental results of PZT at position ① in Fig. 1

3.6　理论和实验结果对比

图 7 实线为相位调制噪声仿真结果，“○”为补偿干涉仪与传感器相邻的实验结果，“*”为补偿干涉仪与传感器分开的结果。从图 7 中可以看出，理论和实验结果符合得较好，两种结构的相位调制噪声大小与相应的匹配光程差一致。

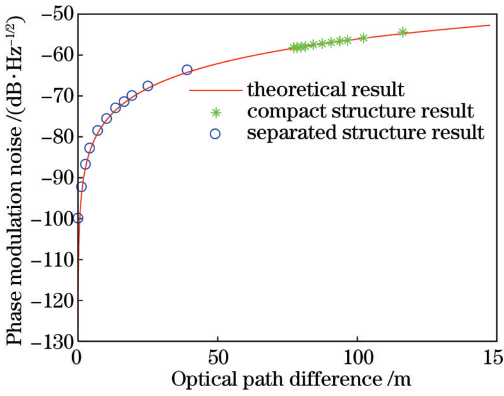

图 7　理论和实验结果对比图

Fig. 7　Comparison of theoretical and experimental results

3.7　相位噪声本底对比图

实验中对紧凑型匹配干涉结构的不同匹配光程差在三个不同频点处的噪声本底对应的相位噪声本底值进行了分析，其分析结果与文献[7]的实验结果一致，如图 8 所示。

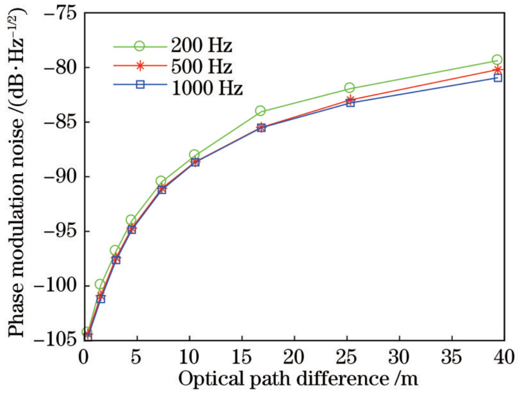

图 8　不同频点相位调制噪声本底对比图

Fig. 8　Comparison of phase modulation noise background at different frequencies

4　结　　论

首先从理论上分析了匹配干涉远程光纤传感系统中补偿干涉仪和传感器不同结构和不同臂差对系统噪声的影响，之后设计实验进行验证，结果表明理论和实验结果符合得较好，所得结论如下：

1)理论分析了补偿干涉仪与传感器相邻与分开时系统相位调制噪声的差异，结果表明两种结构下的系统相位调制噪声幅度相差 $20\lg(\tau_2/\tau)$。

2)当补偿干涉仪与传感器相邻时，该结构的微分作用可以削弱传输光纤上的相位调制噪声和随机噪声，且匹配效果越好，微分作用越明显，同时该结构可以有效抑制返回传输光纤上的相位调制噪声。

3)当补偿干涉仪与传感器分开时，相位调制噪声仅与传感器的臂差有关，与补偿干涉仪臂差或二者的匹配光程差无关。传感器的臂差越大，相位调制噪声也越大。

4)获得了最优的匹配干涉系统结构。在设计 PGC 内调制远程匹配干涉型光纤传感系统时，应对补偿干涉仪进行良好声音振动屏蔽，在满足 PGC 内调制和相位调制对臂差需求的情况下，应减小匹配光程差，同时使补偿干涉仪与传感器相邻，利用这种结构的微分效应削弱传输光纤相位调制噪声和低频随机噪声的作用。

参　考　文　献

[1] 廖延彪. 光纤光学[M]. 北京: 清华大学出版社, 2000: 78-91.
Liao Y B. Optical fiber[M]. Beijing: Tsinghua University Press, 2000: 78-91.

[2] Kirkendall C K, Dandridge A. Overview of high performance fibre-optic sensing[J]. Journal of Physics D: Applied Physics, 2004, 37(18): R197-R216.

[3] Yuan L B, Wen Q B, Liu C J, et al. Twin multiplexing strain

sensing array based on a low-coherence fiber optic Mach-Zehnder interferometer[J]. Sensors and Actuators A: Physical, 2007, 135(1): 152-155.

[4] Chang C C, Sirkis J. Multiplexed optical fiber sensors using a single Fabry-Perot resonator for phase modulation[J]. Journal of Lightwave Technology, 1996, 14(7): 1653-1663.

[5] Lo Y L, Chuang C H. Differential optical fiber refractometer based on a path-matching differential interferometer with temperature compensation[J]. Applied Optics, 2001, 40(21): 3518-3524.

[6] Sato R, Saito S. Expansion of dynamic range in interferometric fiber optic hydrophone[J]. Japanese Journal of Applied Physics, 2013, 52(1R): 012501.

[7] Zhou H J, Chen W, Meng Z, et al. Phase noise characteristics of narrow-linewidth fiber laser and laser diode in unbalanced interferometers[J]. Chinese Optics Letters, 2013, 11(2): 021401.

[8] 张岩. 匹配干涉型光纤水听器阵列噪声特性研究[D]. 长沙: 国防科技大学, 2015: 36-42.
Zhang Y. Research on noise character based on matched interferometric fiber optic hydrophone array[D]. Changsha: National University of Defense Technology, 2015: 36-42.

[9] 廖延彪, 苑立波, 田芊. 中国光纤传感 40 年[J]. 光学学报, 2018, 38(3): 0328001.
Liao Y B, Yuan L B, Tian Q. The 40 years of optical fiber sensors in China[J]. Acta Optica Sinica, 2018, 38(3): 0328001.

[10] 苑立波, 童维军, 江山, 等. 我国光纤传感技术发展路线图[J]. 光学学报, 2022, 42(1): 0100001.
Yuan L B, Tong W J, Jiang S, et al. Road map of fiber optic sensor technology in China[J]. Acta Optica Sinica, 2022, 42(1): 0100001.

[11] 孟洲, 陈伟, 王建飞, 等. 光纤水听器技术的研究进展[J]. 激光与光电子学进展, 2021, 58(13): 1306009.
Meng Z, Chen W, Wang J F, et al. Research progress of fiber optic hydrophone technology[J]. Laser & Optoelectronics Progress, 2021, 58(13): 1306009.

[12] 王力, 王永杰, 于非, 等. 光纤传感技术在物理海洋观测领域的应用研究[J]. 激光与光电子学进展, 2021, 58(13): 1306014.
Wang L, Wang Y J, Yu F, et al. Application of optical fiber sensing technology in the field of physical ocean observation[J]. Laser & Optoelectronics Progress, 2021, 58(13): 1306014.

[13] Chen W, Meng Z, Zhou H J, et al. Stimulated Brillouin scattering-induced phase noise in an interferometric fiber sensing system[J]. Chinese Physics B, 2012, 21(3): 034212.

[14] Anderson B, Flores A, Holten R, et al. Comparison of phase modulation schemes for coherently combined fiber amplifiers[J]. Optics Express, 2015, 23(21): 27046-27060.

[15] 曹春燕, 胡正良, 熊水东, 等. 光纤水听器远程传输中相干瑞利噪声的抑制[J]. 中国激光, 2012, 39(10): 1005005.
Cao C Y, Hu Z L, Xiong S D, et al. Suppression of Rayleigh scattering induced coherent noise in remotely interrogated fiber-optic hydrophones[J]. Chinese Journal of Lasers, 2012, 39(10): 1005005.

[16] Cranch G A, Dandridge A, Kirkendall C K. Suppression of double Rayleigh scattering-induced excess noise in remotely interrogated fiber-optic interferometric sensors[J]. IEEE Photonics Technology Letters, 2003, 15(11): 1582-1584.

[17] Hu X Y, Chen W, Tu X B, et al. Theoretical and experimental study of suppressing stimulated Brillouin scattering and phase noise in interferometric fiber sensing systems with phase modulation[J]. Applied Optics, 2015, 54(8): 2018-2022.

[18] Cranch G A, Kirkendall C K, Daley K, et al. Large-scale remotely pumped and interrogated fiber-optic interferometric sensor array[J]. IEEE Photonics Technology Letters, 2003, 15(11): 1579-1581.

[19] Cranch G A, Nash P J. Large-scale multiplexing of interferometric fiber-optic sensors using TDM and DWDM[J]. Journal of Lightwave Technology, 2001, 19(5): 687-699.

[20] Dandridge A, Tveten A B, Giallorenzi T G. Homodyne demodulation scheme for fiber optic sensors using phase generated carrier[J]. IEEE Journal of Quantum Electronics, 1982, 18(10): 1647-1653.

[21] Dandridge A, Tveten A B. Phase noise of single-mode diode lasers in interferometer systems[J]. Applied Physics Letters, 1981, 39(7): 530-532.

Influence of Path-Matched Differential Interference Structure on Noise of Remotely Interrogated Optical Fiber Sensing System

Tang Qiyong[1*], Cao Chunyan[2**], Xia Xingyu[1], Liu Guobin[1], Zhao Fan[1], Sheng Jingchao[1], Guo Jinyi[1]

[1] *Unit* 63893 *of the Chinese People's Liberation Army, Luoyang* 471000, *Henan, China*;
[2] *College of Meteorology and Oceanography, National University of Defense Technology, Changsha* 410073, *Hunan, China*

Abstract

Objective The interferometric optical fiber sensing (OFS) system based on the beam interference principle has the advantages of a wide working frequency band, small volume, and invulnerability to electromagnetic interference. It is of great significance for national security, oil and natural gas exploration, seismic detection and warning, etc. The Mach-Zehnder and Michelson interferometer structures are commonly used in practical OFS systems. Among them, the OFS system with path-matched differential interference (PMDI) is one of the research hotspots for its simple structure, high optical energy utilization rate, and flexible demodulation schemes. Up to now, the interference of the conventional PMDI structure is usually perfectly matched, and the compensation interferometer is located at the emitter or receiver end. This structure has the following problems when it is applied to the remotely interrogated OFS system: 1) the pickup noise accumulates along the remote transmission fiber and will be finally converted into great system noise by the optical differential effect; 2) in the remotely interrogated OFS system, optical frequency modulation or phase modulation (PM) is required to suppress the phase noise induced by stimulated Brillouin scattering (SBS). As the interference of the conventional PMDI structure is usually perfectly matched, external carrier signals cannot be directly loaded into the interferometer, which means the conventional PMDI structure is no longer applicable. Although the carrier signals could be loaded on one arm of the interferometer by a piezoelectric transducer (PZT) or an electro-optic modulator (EOM), this will destroy the passive property of the system and also introduce some electrical noise. In view of the above-mentioned defects, the paper proposes an improved PMDI structure for remotely interrogated OFS applications. Through numerical simulation and experimental verification, the optimal PMDI structure for remotely interrogated OFS systems is obtained. We hope that the conclusions drawn in this paper can provide a theoretical and experimental reference for the comprehensive design and noise suppression of remotely interrogated OFS systems.

Methods This paper studies the influence of the PMDI structure on the noise of a remotely interrogated OFS system with phase generated carrier (PGC) techniques. Firstly, the influence of different PMDI structures on PM noise is analyzed. Through numerical simulation and experimental verification, the optimal PMDI structure for the remotely interrogated OFS system is obtained. Then, the influence of different path-matched differences on the PM noise of the system is studied. Finally, the phase noise background with different optical path-matched differences is measured experimentally.

Results and Discussions The differences in the system PM noise when the compensation interferometer and the sensor are adjacent and separated are analyzed theoretically. The results show that the amplitude difference in the system PM noise under the two structures is $20\lg(\tau_2/\tau)$. When the compensation interferometer is adjacent to the sensor, noise caused by environmental disturbance to the lead fiber can be greatly reduced by the optical differential effect (Fig. 2). When the compensation interferometer is separated from the sensor, the PM noise is only related to the OFS arm difference, which is independent of the arm difference of the compensation interferometer or their optical path-matched difference. When the OFS arm difference increases, the PM noise also rises (Fig. 3).

Conclusions This paper first theoretically analyzes the influence of different structures and arm differences of the compensation interferometer and the sensor on the noise in the remotely OFS system of PMDI. Then, it designs an experiment for verification. The results show that the theory is in good agreement with the experiment, and the following conclusions are drawn.

1) The differences in the system PM noise when the compensation interferometer and the sensor are adjacent and separated are analyzed theoretically. The results reveal that the amplitude difference in the system PM noise under the two structures is $20\lg(\tau_2/\tau)$.

2) When the compensation interferometer is adjacent to the sensor, the PM noise and random noise on the transmission fiber can be greatly reduced by the optical differential effect. A smaller path-matched difference indicates a more significant optical differential effect, and the returned PM noise on the transmission fiber can be effectively suppressed.

3) When the compensation interferometer is separated from the sensor, the PM noise is only related to the arm difference of the sensor, which is independent of that of the compensation interferometer or their optical path-matched difference. As the arm difference of the sensor grows, the PM noise also increases.

4) The optimal PMDI structure is obtained. In the design of a remotely interrogated OFS system with internal modulation of PGC, the compensation interferometer should be well shielded from sound and vibration. When the requirements of the internal modulation of PGC and PM for arm differences are satisfied, the optical path-matched difference should be as small as possible. Meanwhile, the compensation interferometer should be adjacent to the sensor. The optical differential effect of this structure can be used to suppress the PM noise and low-frequency random noise on the transmission fiber.

Key words fiber optics; optical fiber sensing; path-matched differential interference; optical path-matched difference; phase modulation noise